Aminated hydroximoyl camelthorn residues as a novel adsorbent for extracting Hg(II) from contaminated water: studies of isotherm, kinetics, and mechanism

A. Hashem[a]*, A. J. Fletcher[b] ,M. El-Sakhawy[c] , Latifa A. Mohamed[d], and S. Farag[a]

*Email: (alihashem2000@yahoo.com)

[a] National Research Center, Textile Research Division, Dokki, Cairo, Egypt.

[b] Department of Chemical and Process Engineering, University of Strathclyde, 75 Montrose Street, Glasgow, G1 1XJ, UK.

[c] Cellulose and Paper Department, National Research Centre, 33 El-Bohouth Str., P.O. 12622, Dokki Giza, Egypt.

[d] Microbial Chemistry Department, National Research Center, Dokki, Cairo, Egypt.

Abstract

Camelthorn (CT), a desert plant, has been utilized as an adsorbent material for the extraction of Hg(II) ions from aqueous solution after grafting with acrylonitrile followed by amination with hydroxylamine hydrochloride in basic medium to obtain aminated hydroximoyl camelthorn (AHCT). AHCT were found to exhibit excellent adsorption capacity over a wide range of Hg(II) concentration. The surface functional groups and morphology of aminated hydroximoyl camelthorn were determined. The influences of time (0-60 min), pH (2-6), and dose (0.3-8 g/L) were also evaluated. The adsorption data were analyzed using the Langmuit, Freundlich and Temkin tr models at 30°C using nonlinear regression analysis. The maximum adsorption capacity (q_{max}) of Hg(II) onto AHCT was 272.9 mg/g at an initial pH of 6 and a temperature of 30°C and the Freundlich constants, K_F and n, at 30 ^oC were found to be 25.47 mg/g and 3.2, respectively. The value of n (3.2), which being in the range 0-10 indicate that adsorption of Hg(II) ions onto AHCT is favorable. Various kinetics models including the pseudo-first-order, pseudo-second-order and intraparticle diffusion models have been applied to the experimental data to predict the adsorption kinetics. Kinetic study was carried out by varying initial concentration of Hg(II) at constant temperature and it was found that pseudo-second-order rate equation was better obeyed than pseudo-first-order and intraparticle diffusion supporting that chemisorption process was involved. The examination of R^2 values and error analysis method (ARE) showed that the Langmuir model provide the best fit to experimental data than other isotherms and follow the following order: Langmuir > Freundlich > Temkin.

The results revealed that the aminated hydroximoyl camelthorn-Hg(II) ions adsorption system was promoted by the high density of active sites and the adsorption process is independent of the adsorbent surface area.

Consequently, aminated hydroximoyl camelthorn residues can offer an effective method of Hg (II) ion removal from aqueous solutions, demonstrating its potential role in water remediation processes.

Keywords: Adsorption; mercury (II) ions; kinetics; isotherms; camelthorn; adsorbent.

1. Introduction

Sound utilize of water resources appears to be one of the world's urgent environmental problems, the solution to which largely lies in treating wastewater that comes from human activities in different areas: industries (such as battery, tannery, mining, metallurgical, chemical, and nuclear), agriculture, shipping and others. It is particularly important to control levels of heavy metals which are one of the most biologically dangerous and toxic components of wastewater effluents [1]. In particular, water contamination is an area of concern because heavy metal pollution causes different diseases. Several methods have been created to successfully remove heavy metals from wastewater. Typical treatment strategies for the extraction of heavy metal ions in wastewater include ion exchange, chemical precipitation, electrochemical methods, chemical coagulation, membrane filtration and biosorption [2].

Mercury is considered to be highly toxic, and is deemed a hazardous pollutant; the World Health Organization recommends a permissible of mercury content in drinking water of 6 μg L^{-1}[3, 4]. Long term exposure to mercury can result in renal, pulmonary or cardiovascular disease [5], while the development of the foetal nervous system may be impaired if a mother consumes seafood containing high levels of MeHg during pregnancy[6]. The ecological and health hazards presented by uncontrolled release of Hg(II) have fostered significant research effort into a comprehensive method of remediation. As for other inorganic species, adsorption has frequently been used to remove Hg(II) ions from aqueous solutions[7-9]. Due to their tailorable textural characteristics, including pore diameter, extensive surface area, and ease of manufacture activated carbons, derived from biomass, are the most prolific adsorbents used in such applications. Within this family of materials, agricultural waste materials, and their associated carbonaceous forms, offer great potential to extract heavy metals from wastewater [10]. Use of such raw agricultural waste

as alternatives to comparatively expensive activated carbons has attracted attention due to their low-cost of processing, wide availability, and favourable physicochemical properties of this free resource. Consequently, agricultural wastes have become one of the most used materials for the adsorption of pollutants, such as heavy metals, oils, dyes and toxic salts from water, as a result of the high adsorption capacity that the inherent cellulose and lignin exhibit for these pollutants [11, 12]. In recent years, modified cellulose has been investigated widely for heavy metal adsorption. The modification of cellulosic materials via the addition of functional groups to the hydroxyl groups present on the backbone of cellulose can enhance its adsorption capacity toward metal ions [13]. camelthorn (CT), is a perennial thorny shrub native to desert regions with a wide soil tolerance, flourishing in salty, sandy, rocky and arid soils; the plant is utilised in a range of applications including topical medical treatments and as a sweetener. While native to regions extending from the Mediterranean to Russia, it has been introduced to several other countries, where it is considered an invasive species, most notably in Europe, North America and Oceania. The main plant grows to a height of ~1 m, however, the roots extend up to 5-7 m in depth, with penetration depths up to 15 m observed in extreme cases [14, 15] as the plant seeks groundwater in its hyper-arid environment. Combined with a lateral spread of more than 8 m [16], this means that removal of the shrub results in significant biomass, the majority comprising root material with a high-cellulosic content. This makes CT an excellent candidate for use in heavy metal ion remediation, with scope for further enhancement of the exhibited properties via surface modification. In the present study, modified CT was used as a new adsorbent for adsorption of Hg(II) after grafting with acrylonitrile and subsequent reaction with hydroxylamine hydrochloride to from aminated hydroximoyl camelthorn (AHCT). Such adsorbents have not been used previously, this work presents full characterization of these new materials and insights into the mechanism of adsorption and kinetic models obeyed for Hg(II) ion adsorption from aqueous systems.

2. Materials and methods

2.1. Materials

The sample of CT used here was obtained from the Martouh desert, Egypt. Due to the high cellulosic content of the root material, this was separated from the stems and leaves, the latter being discarded. The root material was washed with copious amounts of distilled water to remove any particles adhered to the surface, before drying at 80oC in an electric oven for 24 h, and

subsequent grinding and sieving to a particle size of 50–120 μm. All reagents used in this study, acrylonitrile, ammonium cerium(IV) nitrate, mercuric acetate, sodium hydroxide, EDTA, nitric acid, sodium carbonate, acetone, and ethyl alcohol were all laboratory grade chemicals, supplied by Merck, Germany.

2.2. Preparation of adsorbent

Grafting of CT

Varying amounts of acrylonitrile were grafted onto the CT surface according to the reported method [17] of follows: 4 g of root material was added to a predetermined quantity of acrylonitrile (7.5 to 45 mmol L^{-1}) in a 100 mL of Erlenmeyer flask, pre-equilibrated, in a thermostatic water-bath, to a pre-selected temperature, in the range 40 to 70 ^{o}C. Ammonium cerium(IV) nitrate was added as an initiator and the reaction mixture agitated thoroughly at the start of the reaction, and periodically throughout the polymerization process. The resulting homopolymer of poly-acrylonitrile and CT (CT-PAN) was removed from the reaction mixture via Soxhlet extraction, using N, N-dimethylformamide, over a period of 24 h. Results are reported in terms of liquor ration, which represents the ratio between the total volume of the reaction solution (ranging from 10 to 50 mL) and the mass of cellulosic material used, here set at 4 g; for example a liquor ratio of 2.5 denotes a mass of 4 g and, by mathematical solution, a total reaction volume of 10 mL.

Preparation of AHCT

AHCT was prepared according to the reported method [18] as follows: a solution of free hydroxylamine in methanol-water (5:1) was prepared from its hydrochloride salt. Accurtely, 4.5g of hydroxylamine hydrochloride was dissolved in 30 ml of methanol-water (5:1) mixture. The HCl of NH_2OH was neutralized by NaOH solution and the precipitate of NaCl was removed by filtration. The pH of the reaction was adjusted to pH 8- 8.5 by controlling with NaOH solution (0.1M).

The above-prepared free hydroxylamine solution was added to 4g of the poly(acrylonitrile)-grafted camelthorn residues a flask fitted with condenser. The aminated hydroximoyl camelthorn (Scheme 1) was prepared at 345 K for 8h. The aminated hydroximoyl camelthorn was filtered off, thoroughly washed with water for different times to remove the unreacted hydroxylamine and then dried at 80C for 5h.

2.3. Determination of Nitrogen Content

The percentage of nitrogen content of PAN-grafted CT samples was determined using the micro-Kjeldahl method [19]. In brief, the sample to be analyzed is heated with concentrated H_2SO_4 at 633–683 K, in the presence of a K_2SO_4/Na_2SO_4 (1:10) catalyst mixture, to achieve boiling of the resulting solution and oxidatively decompose the organic sample to produce ammonium sulphate; excess NaOH (10 N) is added to this product and the mixture heated with an attached condenser. This produces ammonia gas, which is bubbled through a solution of boric acid to give ammonium borate. Finally the nitrogen content of the sample is measured via titration using HCl acid (0.01 N) and methyl red indicator.

2.4. Batch Adsorption Studies

A weighed quantity of adsorbent (0.03 g) was added to 100 mL of mercury acetate solution (100–1000 mg L^{-1}) in a 125 mL Erlenmeyer flask. 0.1 M HNO_3 or 0.1 M NaOH was added dropwise to adjust pH values and the mixture shaken at a constant speed (150 rpm, Julabo LABORTECHNIK GMBH D-7633 Seelbach/Germany) at 303 K for 2 h, before filtering to separate out the metal ion solution. The concentration of Hg(II) ions was measured before and after adsorption, using direct titration with a standard EDTA solution (0.0005 M).

The amount of adsorbed Hg(II) at equilibrium, q_e (mg g^{-1}) was calculated using:

$$q_e = \frac{V(C_o - C_e)}{W} \qquad 1$$

While the percentage removal was calculated via:

$$\text{Removal } \% = \frac{(C_o - C_e)}{C_o} \cdot 100 \qquad 2$$

where C_o and C_e (mg L^{-1}) are the initial metal concentration and metal concentration at equilibrium, respectively; W (g) is the weight of adsorbent used, and V is the volume of Hg(II) solution (0.1 L).

2.5. Adsorbent characterisation

The CT residues, CT-PAN, AHCT and AHCT loaded with Hg(II) ions were characterised using Fourier Transform infrared spectroscopy (FTIR), and subsequent assignment of the vibrational frequencies of different functional groups present in the adsorbent structure and any resulting

bonds between mercury ions and the adsorbent surface. Averaged FTIR spectra of the samples were obtained over a wavelength range of 4000–400 cm^{-1} (scan interval: 1 cm^{-1}, number of scans: 120) using KBr discs containing ~2-10 mg of sample in ~300 mg of KBr, using a Perkin–Elmer Spectrum 1000 spectrophotometer. The morphology of the AHCT adsorbent was investigated using scanning electron microscopy (SEM); the adsorbent samples were coated with chromium on carbon tape, prior to analysis (TESCAN CE; Type: VEGA 3 SBU; No.:117-0195- Czech Republic). Images were taken at 2000× magnification. Energy-dispersive X-ray (EDX) analysis was performed for the AHCT adsorbent, using a dispersive X-ray fluorescence (EDX) spectrometer Model (Oxford) attached to the SEM Model JEOL-JSM-5600, to allow determination of the presence or absence of mercury. The textural characteristics of the AHCT adsorbent were investigated via nitrogen adsorption at 77 K using an Autosorb I. Analysis of the data obtained was performed using Brunauer-Emmet-Teller theory; mesopore volume, external surface area, and mesopore surface area were determined using the t-plot method; while the Barrett-Joyner-Halenda technique was used to calculate the average pore width and determine the pore size distribution. The pH at point of zero charge (pHpzc) of the AHCT adsorbent was evaluated by separately adding 100 mL of 0.01 N NaCl to a series of conical flasks and adjusting the pH of the suite of solutions, using 0.01 N HCl and 0.01 N NaOH, to pre-selected values within the range 2 to 12. Once equilibrium was established for each solution, the initial pH was recorded, whereafter, ~100 mg of the AHCT adsorbent was dispersed in each conical flask and incubated for 24 h to obtain the final pH. The initial and final pH values were plotted, with the intersection points of the plots designated as the pHpzc of the adsorbent.

2.6. Error analysis

The suitability and accuracy of the suite of kinetic and isotherm models used in to fit the data obtained in this study were evaluated using the coefficient of determination (R^2) and absolute relative error (ARE) [20], shown in Equations 3 and 4, respectively. ARE and R^2values close to unity were used as criteria for selection of the kinetic and isotherm models that best described the experimental data.

$$\boldsymbol{R^2} = \frac{\sum\left(\boldsymbol{q_{ecal}} - \boldsymbol{q_{mexp}}\right)^2}{\sum\left(\boldsymbol{q_{ecal}} - \boldsymbol{q_{mexp}}\right)^2 + \left(\boldsymbol{q_{ecal}} - \boldsymbol{q_{mexp}}\right)^2} \qquad 3$$

$$ARE = \frac{100}{n}\sum_{i=1}^{n}\left[\frac{q_{e,i,cal} - q_{e,i,exp}}{q_{e,i,exp}}\right] \quad (4)$$

where n, q_{exp}, and q_{cal} are the range of input data, experimental, and calculated uptake of Hg(II) ions, respectively.

3. Results and Discussion

3.1. Adsorbent characterization

The FT-IR spectra of raw CT residues, PAN-CT, AHCT and AHCT loaded with Hg(II) ions are shown in Figure 1. The difference in the fingerprint peaks for the samples confirm successful grafting, amination and adsorption processes. Figure 1a shows a broadband at 3370 cm^{-1}, characteristic of hydroxyl groups, as expected for the cellulosic structure of CT. The band at 2953 cm^{-1} can be ascribed to C–H stretching vibrations, while the bands observed at 1749 and 1051 cm^{-1} are attributed to ether C=O and C–O stretching, respectively. Figure 1b shows the appearance of a new, sharp peak at 2249 cm^{-1}, characteristic of cyanide groups, which are expected from the grafting of acrylonitrile to CT. The spectrum also exhibits a broad band at 3401 cm^{-1} due to hydrogen bonding between the –OH group of CT and the tertiary amine groups of the grafted chains of PAN-CT. The FT-IR spectra shown in Figure 1c shows a narrowing and weakening of the cyanide group peak at 2252 cm^{-1}; these results clearly indicate the conversion of cyanide groups to hydroximoyl amine groups through treatment with hydroxylamine. Finally, Figure 1d shows a small shift in the absorbance peaks for Hg (II) ion loaded AHCT compared with the other three materials. The broadband observed at 3382 cm^{-1} shifts to 3390 cm^{-1}, while the peaks at 2960 and 1679 cm^{-1} shift to 2953 and 1681 cm^{-1}, respectively. The peak observed at 1075 cm^{-1} was shifted to 1078 and 1059 cm^{-1}. Such shifts, attributable to the coordination of Hg(II) ions, have been observed previously [21].

The morphology of AHCT, as determined by SEM, is presented in Figure 2a and reveals a disordered and agglomerated material with several pore types. There are no significant changes in adsorbent morphology after adsorption of Hg(II) ions (Figure 2b), indicating that AHCT is a robust adsorbent with favourable potential for commercialisation. EDX spectra of AHCT loaded with Hg(II) ionsshows a sharp peak for elemental Hg, present at 9% of the surface composition, and confirming the adsorption of Hg(II) ions onto the surface of AHCT.

The textural characteristics of AHCT were determined via N_2 sorption, which showed a very low BET surface area (6 m^2 g^{-1}) with a similarly small total pore volume (0.01 cm^3 g^{-1}); the material can be categorised as mesoporous with an average pore width of 7 nm [22], which is useful for aqueous phase applications, allowing mass transport and adsorption of Hg(II) ions. The low BET surface area is expected due to the natural precursor used and the additional steps of polymeric grafting and conversion to AHCT. While the surface area of AHCT is relatively low, this may not negatively impact the adsorption capacity, which may be related to the high density of active surface functional groups, and similar studies, on relatively high metal adsorption on low specific surface area adsorbents, have been reported previously in the literature [4, 23].

3.2. Factors affecting grafting reaction

3.2.1. Effect of reactant species

Figure 3 shows the effect of liquor ratio on the resulting nitrogen content of CT residues grafted with AN. It can be seen increasing liquor ratio, from 2.5 to 12.5, results in a decrease in the amount of nitrogen incorporated into these samples (4.1 to 1.3%). However, all conditions show an increase in nitrogen content compared with raw CT residues, which contain 0.3 wt% nitrogen. This demonstrates that a liquor ratio of 2.5 is the optimal ratio used here by providing the most suitable environment for reactant collision [24]. It should be noted that there is a limiting minimum amount of solution that can be used so additional improvement in this parameter would be limited.

The nitrogen contents of modified CT materials, as a function of ammonium cerium(IV) nitrate concentration, are shown in Figure 4. It is evident that, by increasing the concentration of ammonium cerium(IV) nitrate from 2.5 to 5 mmol L^{-1}, the percentage of nitrogen present in the grafted samples increases (3.2 to 4.1%). However, additional increase in the concentration of ammonium cerium(IV) nitrate results in a decrease in the nitrogen content of PAN-CT to levels below that produced by 2.5 mmol L^{-1}. The initial increase observed for this parameter is probably due to increased initiation of the grafting process, where after, higher concentrations, above 5 mmol L^{-1}, may cause an increase in radical cellulose CT before addition to acrylonitrile, as well as the formation of homopolymers causing a decrease in grafting onto CT itself [25].

By selecting the optimum concentration of ammonium cerium(IV) nitrate at 5 mmol L^{-1}, the effect of acrylonitrile monomer concentration was investigated. Figure 5 shows the variation in

nitrogen content versus monomer concentration. There is a clear trend of increasing nitrogen incorporation with increasing acrylonitrile concentration (1.7 to 4.9%), which is likely due to the increased availability of acrylonitrile molecules to react with CT residues at higher concentrations. The cellulosic hydroxyls will be immobile on the CT residue surfaces, hence, these grafting sites, and their reaction, would depend on the availability and proximity of acrylonitrile molecules for the reaction [25] .

3.2.2. Effect of reaction conditions

Figure 6 shows the effect of reaction temperature on the nitrogen content of grafted samples. It can be seen that, when the polymerization temperature increased modestly from 40 to 50 ^{o}C, the nitrogen content increased significantly from 2.9 to 4.3%. Additional increase in reaction temperature does not enhance the grafting process but rather results in a decrease in nitrogen content.

The observed increase in nitrogen content at lower temperatures may be related to the favorable effect of temperature on (a) the diffusion of AN on MT residue cellulose structure;(b) the swellability of cellulose, (c) the ceric-cellulose complexes and its further dissociation, and (d) the mobility and collision of AN molecules with cellulose macro- radicals to initiate grafting. On the other hand, the decrease in percentage nitrogen of the grafted samples at temperatures above 50 ^{o}C could be attributed to faster termination rates and higher range of the formation of homopolymers at higher temperatures, as well as the catalytic effect of temperature on the grafting reaction [25].

Using the optimised reaction temperature of 50 ^{o}C, the effect of reaction time on nitrogen content was studied and the results are presented in Figure 7. The percentage of nitrogen in the grafted samples increases from 2.1 to 4.25% by increasing the duration of the reaction from 30 to 120 minutes and remained at about the same level for higher reaction times. The increase in the percentage of grafted samples of nitrogen by increasing the length of time could be correlated with the beneficial effect of time on (a) the formation of ceric-cellulose complex and its further dissociation and development of CT cellulose macro-radicals capable of initiating grafting; (b) the mobility and diffusion of AN molecules from the aqueous phase to the cellulose phase and (c) the spread of the graft [25] .

3.3. Factors affecting Hg(II) adsorption onto AHCT

3.3.1. Point of zero charges (pHpzc) and the effect of pH

Figure 8a shows the pHpzc results obtained for the surface of the AHCT adsorbent, allowing determination of the pH at which this surface has a neutral charge, which is pH 7 in this case. This indicates that the surface of AHCT is neutral in nature; when the pH value of the solution is higher than the pHpzc, i.e. the whole basic range in this case, then the surface charge of adsorbent will be negative and the system will favour the binding of cations and acidic pH values, lower than the pHpzc, will result in a positive surface charge making adsorption of cations unfavourable [26]. [Shifted]

As stated above, Figure 8a shows that the pHpzc of the AHCT adsorbent is 7; consequently, with adsorption of cations thereby favoured in acidic conditions, the effect of pH on the adsorption of Hg(II) ions by AHCT, in the range pH 2–6, was studied for an initial Hg(II) ion concentration of 300 mg L^{-1}. The results obtained are shown in Figure 5a, and the adsorption of Hg(II) is seen to increase from 23.7 to 178.4 mg g^{-1} with increasing pH, reaching a maximum at pH 6. At high acidity the adsorbent surface will be covered with H_3O^+ ions, and Hg(II) ions would need to compete with these other cations for adsorption sites. The increase in pH to a value of 6, causes the competing effect of H_3O^+ to be diminished, and the positively charged Hg(II) ions are able to adsorb more easily on the freely available binding sites of the adsorbent [27], which appears to be counterintuitive to the pHpzc results discussed above. The pH of 6,which is lower than the pHpzc, results in the adsorbent surface being predominantly positive; this is a result of the protonation of the nitrogen atoms in the amino groups introduced onto the surface of PAN-CT via reaction with hydroxylamine. This positive surface would be reasoned to undergo electrostatic repulsion with the Hg(II) cations in solution [28], making adsorption unfavourable, however, the adsorption mechanism for Hg(II) ions can alternatively be attributed to the formation of metal complexes with the nitrogen in the amine groups of the AHCT rather than direct interaction with the cellulosic backbone. In addition, cations may interact with the oxygen atoms of the hydroxyl groups on the AHCT structure, dependent on solution pH.

3.3.2. Effect of adsorbent dose

It has been previously observed, in many studies, that adsorbent dose influences the uptake of target species from solution, including metal ions. The effect of adsorbent dose on the adsorption

capacity of AHCT for Hg(II) ions was studied at pH 6, using adsorbent doses in the range 0.3–8 g L^{-1}, and an initial metal ion concentration of 300 mg L^{-1} (Figure 9). It can be seen that the adsorption capacity (q_e) of Hg(II) ions, per gram of adsorbent (mg g^{-1}), decreased from 175 to 37 mg g^{-1} with increasing adsorbent dose, up to 8 g L^{-1}. The decrease in adsorption capacity with increasing adsorbent dose, while counterintuitive, can be attributed to the high number of unsaturated adsorption sites, hence the decrease per unit mass, as well as overlap of adsorption sites, and overcrowding of the adsorbent particles, as has been observed previously for Hg(II) ion adsorption [21].

3.3.3. Effect of contact time

The effect of contact time on the adsorption capacity of AHCT towards Hg(II) ions, at initial adsorptive concentrations in the range of 200 to 800 mg L^{-1}, is shown in Figure 10. The capacity of AHCT to adsorb Hg(II) ions increased with increasing contact time, achieving equilibrium within 60 min for all initial concentrations, after which plateaus are observed and no further improvement is observed. This equilibrium time is relatively short [29], which is an important consideration in the development of an economically viable wastewater treatment system.

3.3.4. Isothermal analysis of Hg(II) ion adsorption on AHCT

Adsorption isotherms offer insight into the interactions that take place between an a selected adsorbate and an adsorbent; the resulting information that can be obtained from their shape and interpretation/analysis provides scope for optimisation of adsorption systems, particularly the adsorbent species. Evaluation of the equilibrium amount of adsorbate taken up per unit mass, qe (mg g^{-1}), and the adsorbate equilibrium concentration, C_e (mg L^{-1}), provides the information required to plot the associated adsorption isotherm. The maximum uptake capacity for adsorption of Hg(II) ions onto AHCT at 30 ^{o}C was determined using the Langmuir, Freundlich and Temkin models. Parameters and goodness of fit are detailed in Table 1. Each of the three isotherm models selected are based on two parameters, and fits to the experimental isotherm data obtained in this study were evaluated by determining ARE and R^2 values for each model. The calculated isotherm parameters and their corresponding ARE analysis of the parameters and R^2 values are listed in Table 1. The isotherm models are ordered, in terms of best fit to the experimental data, as Langmuir > Freundlich > Temkin. Langmuir being selected as the most appropriate model as it gave the highest R^2 value, as well as the lowest ARE values, indicating that it gave the best

overall fit to the data for adsorption of Hg(II) onto AHCT (Figure 11). The Langmuir isotherm model gave an final equilibrium uptake of 273 mg L^{-1}, and the Freundlich model, marginally less good at describing the experimental data, gave an *n* value of 3.2, which being in the range 0-10 indicates that adsorption of Hg(II) ions onto AHCT is favourable. The value of 1/n < 1 suggests a slight suppression of adsorption at lower equilibrium concentrations. In comparison with other adsorbents reported in the literature for adsorption of mercury, the AHCT adsorbent offers a high degree of affinity for removal of mercury, as shown in Table 2 [8, 30-35]. The equations of all adsorption isotherms [36-38] addressed in this paper are listed in Table 3. The comparison between the experimental data and the data obtained from isotherm models (Figure 11) as well as the constants, R^2 and ARE of isotherm models are listed in Table 1.

3.4. Adsorption kinetics

In addition to studying the equilibrium behaviour of adsorption systems, it is critical to understand their approach to this equilibrium by also studying the kinetics of adsorption, which can provide insight into the mechanism of adsorption. In this work, three models were used to model the kinetics of Hg(II) ion adsorption onto AHCT: pseudo-first-order, pseudo-second-order, and intra-particle diffusion. The kinetic process of the pseudo-first-order is usually considered physical adsorption and is diffusion controlled. The non-linear mathematical form of the pseudo-first-order model [39] is given by:

$$q_t = q_e[1 - exp(-k_1 t)] \qquad 5$$

where q_t is the amount of Hg(II) ions adsorbed (mg g^{-1}) at time t (min), q_e is the amount of Hg(II) ions adsorbed (mg g^{-1}) at equilibrium, and k_1 is the rate constant of adsorption (min^{-1}). The non-linear plots of pseudo first-order of Hg(II) ions onto AHCT at a range of concentrations are shown in Figure 12. The values of k_1, and q_e along with R^2, and ARE were summarised in Table 4.

The pseudo-second order kinetic model [40] can be expressed by:

$$q_t = \frac{k_2 q_e^{2} t}{(1 + k_2 k_e t)} \qquad 6$$

where q_t, q_e and t are as defined above,and k_2 (g mg^{-1} min^{-1}) is the rate constant for adsorption. This model assumes that the rate of adsorption is controlled by the sharing of electrons between

the adsorbent and adsorbate, i.e. a chemical process. The non-linear plots of pseudo second-order adsorption of Hg(II) ions onto AHCT at a range of concentrations are shown in Figure 13. The values of k_2, and q_e along with R^2, and ARE were summarised in Table 4. The results of the statistical regression presented in Table 4 reveals that the pseudo second order model show a high degree of correlation with the experimental data, giving a minimum absolute residual error (ARE) and R^2 values close to unity. This suggests the mechanism of Hg(II) adsorption onto the AHCT adsorbent is controlled by chemisorptions [41].

The overall kinetics of adsorption process, when controlled by intra-particle diffusion [42], can be expressed by:

$$q_t = k_{id} t^{0.5} + q_e \qquad 7$$

where q_t, q_e, and t are as defined above, and k_{id} (mg g^{-1} $min^{1/2}$) is the intra-particle diffusion rate constant. Previous studies report that a plot of q_t vs. $t^{1/2}$ gives multi-linear steps controlled by the adsorption process [3, 43]. The values of the intercept, C , as detailed in Table 4, give an idea about the boundary layer thickness, i.e. the larger the intercept, the greater is the boundary layer effect [44]. The rate of diffusion was determined, as this is the rate controlling step in the adsorption process, which incorporates the transport of adsorbate from the bulk solution to the interior surface of the pores in AHCT. Likely that the transport of metal ions from the solution into the pores of the adsorbent is the rate controlling step in batch experiments, especially with rapid agitation[45]. The rate parameter for intra-particle diffusion, was determined for the six concentrations of Hg(II) used in this study (Figure 14), and the values of kp are listed in Table 4.

The results reveal a two-segment linear plot, indicating that the mechanism of adsorption of Hg(II) on AHCT could be controlled by two or more processes [46, 47], which is in agreement with the fits observed for the pseudo-second-order model. In the first segment, the initial adsorption begins with an initial region of very rapid film diffusion, followed by slower intra-particle diffusion at the second stage, as the system approaches or attains equilibrium. The slope of the plot (Fig. 14) is a rate parameter, which is a characteristic of an adsorption system where intra-particle diffusion is rate controlled. Also, the second segment deviates from the origin, which can be attributed to a difference in the mass transfer rate between the initial and final adsorption stage [48].

The results obtained for all models, suggest that the removal of Hg(II) ions from aqueous solution onto the surface of AHCT may occur via the following (i) chelation between the electron-accepting Hg(II) ions and the electron donating electrons found in the nitrogen and oxygen containing functionalities of AHCT, and (ii) intra-molecular dispersion, involving (a) movement of the adsorbate from the bulk of the solution to the outside of the adsorbent, (b) dispersion of the adsorbate through the boundary layer to the external surface of the adsorbent, (c) adsorption at the dynamic sites on the external surface of AHCT, and (d) intra-particle-diffusion of the Hg(II) particles into the inside pores of the adsorbent.

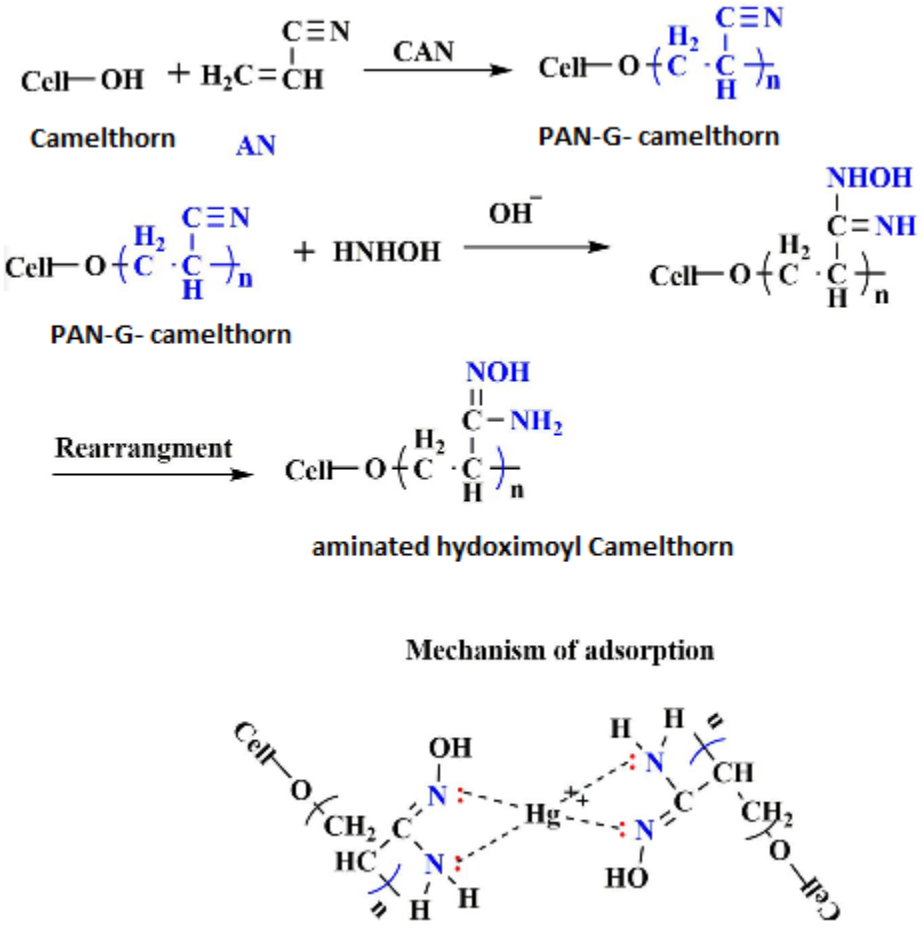

Scheme 1: Schematic presentation of proposed complex structure between AHCT and Hg(II) ions.

4. Conclusions

Camelthorn, CT particles were grafted by treatment with acrylonitrile to obtain poly(AN-grafted camelthorn. Factors affecting the grafting of CT were investigated. These factors were liquor

ratio, ammonium cerium (IV) nitrate concentration, acrylonitrile concentration, reaction time and temperature. The grafted product was modified with hydroxylamine hydrochloride in basic medium to obtain aminated hydroximoyl camelthorn (AHCT). The AHCT samples were characterized by FT-IR spectral analysis, BET surface area, and SEM before and after adsorption of Hg(II). The nitrogen content of CT and AHCT were also determined. The AHCT were utilized for the extraction of Hg(II) ions from aqueous solution by using batch adsorption technique. The results indicated that the adsorption capacity of aminated hydroximoyl camelthorn towards Hg(II) ions was affected by the contact time, adsorbent dose, pH and adsorbate concentration. The data of the adsorption isotherm was tested by the Langmuir, Freundlich and Temkin using non-linear regression technique at 30°C. The results obtained showed that the maximum adsorption capacity according to the Langmuir equation was 272.9 mg/g at 30°C. The kinetics of adsorption of Hg(II) onto aminated hydroximoyl camelthorn have been discussed using three kinetic models, i.e. the pseudo-first-order model, the pseudo-second-order model, and the intraparticle diffusion model using non-linear regression . The adsorption of Hg(II) onto aminated hydroximoyl camelthorn could be well described by the pseudo-second-order kinetic model and intaparticle diffusion models indicating that the mechanism was chemisorptions. The best fitting model was firstly evaluated using two different error functions. The examination of these error estimation methods showed that the Langmuir model provide the best fit for experimental data than other isotherms indicating that the Hg adsorption occurred through the formation of a monolayer sorption.

Consequently, aminated hydroximoyl camelthorn residues offer an effective method of Hg (II) ion removal from aqueous solutions, demonstrating its potential role in water remediation processes.

References

[1] Alexander E. Burakov, Evgeny V. Galunin, Irina V. Burakova, Anastassia E. Kucherova, Shilpi Agarwal, Alexey G. Tkachev, Vinod K. Gupta, Adsorption of heavy metals on conventional and nanostructured materials for wastewater treatment purposes: A review, Ecotoxicology and Environmental Safety 148 (2018) 702–712, doi.org/10.1016/j.ecoenv.2017.11.034

[2] Mi Young Kim, Haein Seo, Tai Gyu Lee, Removal of Hg(II) ions from aqueous solution by poly(allylamine-co-methacrylamide-co-dimethylthiourea), Journal of Industrial and Engineering Chemistry 84 (2020) 82–86, doi.org/10.1016/j.jiec.2019.12.023

[3] H.K. Boparai, M. Joseph, D.M. O'Carroll, Kinetics and thermodynamics of cadmium ion removal by adsorption onto nano zerovalent iron particles, Journal of hazardous materials, 186 (2011) 458-465, doi:10.1016/j.jhazmat.2010.11.029

[4] L. Qi, F. Teng, X. Deng, Y. Zhang, X. Zhong, Experimental study on adsorption of hg (II) with microwave-assisted alkali-modified fly ash, Powder Technology, 351 (2019) 153-158, doi: 10.1016/j.powtec.2019.04.029

[5] Y. Fu, J. Jiang, Z. Chen, S. Ying, J. Wang, J. Hu, Rapid and selective removal of Hg (II) ions and high catalytic performance of the spent adsorbent based on functionalized mesoporous silica/poly (m-aminothiophenol) nanocomposite, Journal of Molecular Liquids, 286 (2019) 110746, doi: 10.1016/j.molliq.2019.04.023

[6] N. Saman, H. Kong, S.S. Mohtar, K. Johari, A.F. Mansor, O. Hassan, N. Ali, H. Mat, A comparative study on dynamic Hg (II) and MeHg (II) removal by functionalized agrowaste adsorbent: breakthrough analysis and adsorber design, Korean Journal of Chemical Engineering, 36 (2019) 1069-1081, doi:10.1007/s11814-019-0285-z

[7] M. Zabihi, A.H. Asl, A. Ahmadpour, Studies on adsorption of mercury from aqueous solution on activated carbons prepared from walnut shell, Journal of hazardous materials, 174 (2010) 251-256, doi: 10.1016/j.jhazmat.2009.09.044

[8] Y. Li, M. Xia, F. An, N. Ma, X. Jiang, S. Zhu, D. Wang, J. Ma, Superior removal of Hg (II) ions from wastewater using hierarchically porous, functionalized carbon, Journal of hazardous materials, 371 (2019) 33-41, doi: 10.1016/j.jhazmat.2019.02.099

[9] S. Zhang, X. Yang, M. Ju, L. Liu, K. Zheng, Mercury adsorption to aged biochar and its management in China, Environmental Science and Pollution Research, 26 (2019) 4867-4877, doi: 10.1007/s11356-018-3945-3

[10] A. Khalil, H. Sokker, A. Al-Anwar, A.A. El-Zaher, A. Hashem, Preparation, Characterization and Utilization of Amidoximated Poly (AN/MAA)-grafted Alhagi Residues for

the Removal of Zn (II) Ions from Aqueous Solution, Adsorption Science & Technology, 27 (2009) 363-382, doi.org/10.1260/026361709790252669

[11] X. Chen, R. Xu, Y. Xu, H. Hu, S. Pan, H. Pan, Natural adsorbent based on sawdust for removing impurities in waste lubricants, Journal of hazardous materials, 350 (2018) 38 45, doi: 10.1016/j.jhazmat.2018.01.057

[12] S. Sirusbakht, L. Vafajoo, S. Soltani, S. Habibi, Sawdust Bio sorption of Chromium (VI) Ions from Aqueous Solutions, Chemical Engineering Transactions, 70 (2018) 1147-1152, doi.org/10.3303/CET1870192

[13] A. Hashem, A. Azzeer, A. Ayoub, The Removal of Hg (II) Ions from Laboratory Wastewater onto Phosphorylated Haloxylon ammodendron: Kinetic and Equilibrium Studies, Polymer-Plastics Technology and Engineering, 49 (2010) 1463-1472, doi.org/10.1080/03602559.2010.496423

[14] H. Oppenheimer, Summer drought and water balance of plants growing in the Near East, Journal of Ecology, 39 (1951) 356-362. doi 10.2307/2257910

[15] L.J. King, Weeds of the world: biology and control, Weeds of the world: biology and control., (1966), doi; ISSN; ISBN

[16] R. Ambasht, Ecological studies of Alhagi camelorum Fisch, Tropical Ecology, 4 (1963) 72-82, doi : 10.1046/j.1365-294X.2003.01773.x.

[17] A. Hashem, A. Abou-Okeil, A. El-Shafie and M. El-Sakhawy, Grafting of High α-Cellulose Pulp Extracted from Sunflower Stalks for Removal of Hg (II) from Aqueous Solution, Polymer-Plastics Technology and Engineering, 45(2006)135–141, DOI: 10.1080/03602550500373790

[18] Luiz Claudio de Santa Maria, Marcia C.V. Amorim, Moˆnica R.M.P. Aguiar,

Pedro Ivo C. Guimara˜esa, Marcos A.S. Costa, Alcino Palermo de Aguiar,

Paulo Roberto Rezende , Marcelo Souza de Carvalho , Fla´via G. Barbos ,

aJuliano M. Andrade , Roberto C.C. Ribeiro, Chemical modification of cross-linked resin based on acrylonitrile for anchoring metal ions, Reactive & Functional Polymers 49 (2001) 133–143, doi.org/10.1016/S1381-5148(01)00068-2

[19] M. Khalil, K.M. Mostafa, A. Hebeish, Graft polymerization of acrylamide onto maize starch using potassium persulfate as initiator, Die Angewandte Makromolekulare Chemie: Applied Macromolecular Chemistry and Physics, 213 (1993) 43-54, doi.org/10.1002/apmc.1993.052130106

[20] S.-C. Tsai, K.-W. Juang, Comparison of linear and nonlinear forms of isotherm models for strontium sorption on a sodium bentonite, Journal of Radioanalytical and Nuclear Chemistry, 243 (2000) 741-746, DOI: 10.1023/A:1010694910170

[21] A. Hashem, A. Al-Anwar, N.M. Nagy, D.M. Hussein, S. Eisa, Isotherms and kinetic studies on adsorption of Hg (II) ions onto Ziziphus spina-christi L. from aqueous solutions, Green Processing and Synthesis, 5 (2016) 213-224, doi:10.1515/gps-2015-0103

[22] M. Thommes, K. Kaneko, A.V. Neimark, J.P. Olivier, F. Rodriguez-Reinoso, J. Rouquerol, K.S. Sing, Physisorption of gases, with special reference to the evaluation of surface area and pore size distribution (IUPAC Technical Report), Pure and Applied Chemistry, 87 (2015) 1051-1069, doi.org/10.1515/pac-2014-1117

[23] M. Hu, H. Tian, J. He, Unprecedented Selectivity and Rapid Uptake of CuS Nanostructures toward Hg (II) Ions, ACS applied materials & interfaces, 29 (2019)19200-19206, doi: 10.1021/acsami.9b04641

]24] A. Hashem, S.M. Badawy, S. Farag, L.A. Mohamed, A.J. Fletcher, G.M. Taha,

Non-linear adsorption characteristics of modified pine wood sawdust

optimised for adsorption of Cd(II) from aqueous systems,

Journal of Environmental Chemical Engineering 8 (2020) 103966, doi.org/10.1016/j.jece.2020.103966

[25] A.Hashem, Ph.D. Thesis: Vinyl graft Copolymerization onto Chemically Modified Starches, Cairo University, 1993.

[26] M. Martín-Lara, F. Hernáinz, M. Calero, G. Blázquez, G. Tenorio, Surface chemistry evaluation of some solid wastes from olive-oil industry used for lead removal from aqueous solutions, Biochemical Engineering Journal, 44 (2009) 151-159, doi.org/10.1016/j.bej.2008.11.012

[27] A. Hashem, Hamdy A. Hammad and Alaauddin Al-Anwar

Chemically modified Retama raetam biomass as a new adsorbent for Pb(II) ions from aqueous

solution: non-linear regression, kinetics and thermodynamics, Green Process Synth 2015; 4: 463–478, **doi** 10.1515/gps-**2015**-0052

[28] H. Chen, Y. Zhao, A. Wang, Removal of Cu (II) from aqueous solution by adsorption onto acid-activated palygorskite, Journal of Hazardous Materials, 149 (2007) 346-354, doi: 10.1016/j.jhazmat.2007.03.085

[29] A. Hashem, H.A. Hussein, M.A. Sanousy, E. Adam, E.E. Saad, Monomethylolated thiourea–sawdust as a new adsorbent for removal of Hg (II) from contaminated water: equilibrium kinetic and thermodynamic studies, Polymer-Plastics Technology and Engineering, 50 (2011) 1220-1230, doi.org/10.1080/03602559.2011.566301

[30] Z. Ding, R. Yu, X. Hu, Y. Chen, Adsorptive Removal of Hg (II) Ions from Aqueous Solutions Using Chemical-Modified Peanut Hull Powder, Polish Journal of Environmental Studies, 23 (2014) 1115-1121,

[31] S. Basha, Z. Murthy, B. Jha, Sorption of Hg (II) from aqueous solutions onto Carica papaya: application of isotherms, Industrial & Engineering Chemistry Research, 47 (2008) 980-986, doi.org/10.1021/ie071210o

[32] A.K. Meena, K. Kadirvelu, G. Mishra, C. Rajagopal, P. Nagar, Adsorptive removal of heavy metals from aqueous solution by treated sawdust (Acacia arabica), Journal of hazardous materials, 150 (2008) 604-611, doi: 10.1016/j.jhazmat.2007.05.030

[33] F.K. Onwu, C.U. Sonde, J.C. Igwe, Adsorption of Hg 2+ and Ni 2+ from aqueous solutions using unmodified and Carboxymethylated granular activated carbon (GAC), American Journal of Physical Chemistry, 3 (2014) 89-95, doi: 10.11648/j.ajpc.20140306.11

[34] T.A. Saleh, Isotherm, kinetic, and thermodynamic studies on Hg (II) adsorption from aqueous solution by silica-multiwall carbon nanotubes, Environmental Science and Pollution Research, 22 (2015) 16721-16731, doi : 10.1007/s11356-015-4866-z

[35] N. Khairi, N. Yusof, A. Abdullah, F. Mohammad, Removal of toxic mercury from petroleum oil by newly synthesized molecularly-imprinted polymer, International journal of molecular sciences, 16 (2015) 10562-10577, doi: 10.3390/ijms160510562

[36] I. Langmuir, The constitution and fundamental properties of solids and liquids. Part I. Solids, Journal of the American chemical society, 38 (1916) 2221-2295, doi: 10.1021/ja02268a002.

[37] H. Freundlich, Über die adsorption in lösungen, Zeitschrift für physikalische Chemie, 57 (1907) 385-470, doi.org/10.1515/zpch-1907-5723

[38] M. Temkin, Kinetics of ammonia synthesis on promoted iron catalysts, Acta physiochim. URSS, 12 (1940) 327-356,doi:10.12691/ijebb-4-2-4

[39] S.K. Lagergren, About the theory of so-called adsorption of soluble substances, Sven. Vetenskapsakad. Handingarl, 24 (1898) 1-39.

[40] Y.-S. Ho, G. McKay, Pseudo-second order model for sorption processes, Process biochemistry, 34 (1999) 451-465. doi: 10.1016/S0032-9592(98)00112-5.

[41] L.R. Somera, R. Cuazon, J.K. Cruz, L.J. Diaz, Kinetics and Isotherms Studies of the Adsorption of Hg (II) onto Iron Modified Montmorillonite/Polycaprolactone Nanofiber Membrane, in: IOP Conference Series: Materials Science and Engineering, IOP Publishing, 540(2019)012005, doi:10.1088/1757-899X/540/1/012005

[42] W.J. Weber, J.C. Morris, Kinetics of adsorption on carbon from solution, Journal of the Sanitary Engineering Division, 89 (1963) 31-60.

[43] E. Unuabonah, K. Adebowale, B. Olu-Owolabi, Kinetic and thermodynamic studies of the adsorption of lead (II) ions onto phosphate-modified kaolinite clay, Journal of Hazardous Materials, 144 (2007) 386-395, doi.org/10.1016/j.jhazmat.2006.10.046

[44] N. Kannan, M.M. Sundaram, Kinetics and mechanism of removal of methylene blue by adsorption on various carbons—a comparative study, Dyes and pigments, 51 (2001) 25-40, doi : 10.1016/S0143-7208(01)00056-0

[45] V. Poots, G. McKay, J. Healy, Removal of basic dye from effluent using wood as an adsorbent, Journal (Water Pollution Control Federation), (1978) 926-935.

[46] F. Marrakchi, M. Ahmed, W. Khanday, M. Asif, B. Hameed, Mesoporous-activated carbon prepared from chitosan flakes via single-step sodium hydroxide activation for the adsorption of methylene blue, International journal of biological macromolecules, 98 (2017) 233-239, doi: 10.1016/j.ijbiomac.2017.01.119.

[47] D. Kołodyńska, P. Hałas, M. Franus, Z. Hubicki, Zeolite properties improvement by chitosan modification—Sorption studies, Journal of industrial and engineering chemistry, 52 (2017) 187-196, doi.org/10.1016/j.jiec.2017.03.043

[48] I. Tsibranska, E. Hristova, Comparison of different kinetic models for adsorption of heavy metals onto activated carbon from apricot stones, Bulgarian Chem Commun, 43 (2011) 370-377,

Tables

Table 1: Isotherm constants obtained for fits of two-parameter isotherm models applied to adsorption data obtained for Hg(II) ions adsorption onto AHCT residues, at 30 ^{o}C

Isotherm Model	**Parameter**	**Value**	**Error Analysis**	**Value**
Langmuir	a_L	0.0035(l/mg)	R^2	0.998
	q_{max}	272.867 (mg/g)	ARE	0.317
	k_L	0.947 (l/g)		
Freundlich	n	3.219	R^2	0.988
	K_F	25.470 (mg/g)	ARE	1.196
Temkin	A_T	0.329 (l/g)	R^2	0.974
	b_T	81.789 (mg/l)	ARE	1.464

Table 2: Comparison of sorption capacities of various adsorbents for Hg(II)

Adsorbent	Adsorption capacity / mg g^{-1}	Reference
Functionalized bagasse-derived carbon	98	[8]
Chemically modified peanut hull	83.3	[25]
Carica papaya	155.63	[26]
Chemically treated sawdust (Acacia arabica)	20.62	[27]
Carboxymethylated granular activated carbon	19.72	[28]
Silica multiwall-carbon nanotubes	163	[29]
Eucalyptus globules bark carbon	4.014	[30]
Aminatedhydoximoyl manna tree (AHMT)	272.9	Present study

Table 3: List of non-linear adsorption isotherm models used

Isotherm	Equation (Non-linear form)	Reference
Langmuir	$q_e = \frac{k_L.C_e}{1 + a_L.C_e}$	29
Freundlich	$q_e = K_F.C_e^{1/n}$	30
Tempkin	$q_e = \frac{RT}{b_T}\ln(A_T C_e)$	31

Table 4: Kinetic parameters for the adsorption of Hg(II) ions onto AHCT at different initial concentrations

Parameters	Co(mg/l)				
	200	300	500	600	800
$q_e$exp (mg/g)	165.0	175.6	228.8	244.8	255.5
Pseudo-first-order					
q_e /mg g^{-1}	154.6	170.7	213.4	229.5	246.2
K_1 / min^{-1}	0.1046	0.101	0.0988	0.097	0.086
R^2	0.995	0.994	0.994	0.994	0.993
ARE	0.559	0.608	0.668	0.672	0.651
Pseudo-second-order					
q_e/mg g^{-1}	170.4	179.9	235.7	253.9	270.2
K_2 / g mg^{-1} min^{-1}	0.0009	0.001	0.001	0.001	0.001
R^2	0.999	0.999	0.999	0.999	0.999
ARE	0.160	0.265	0.220	0.220	0.259
Intra-particle					
k_{id}	6.01	6.90	9.02	9.81	9.15
C	99.1	100.0	130.0	137.6	155.2
R^2	0.992	0.991	0.992	0.992	0.989
ARE	0.740	0.732	0.690	0.721	0.895

Figures

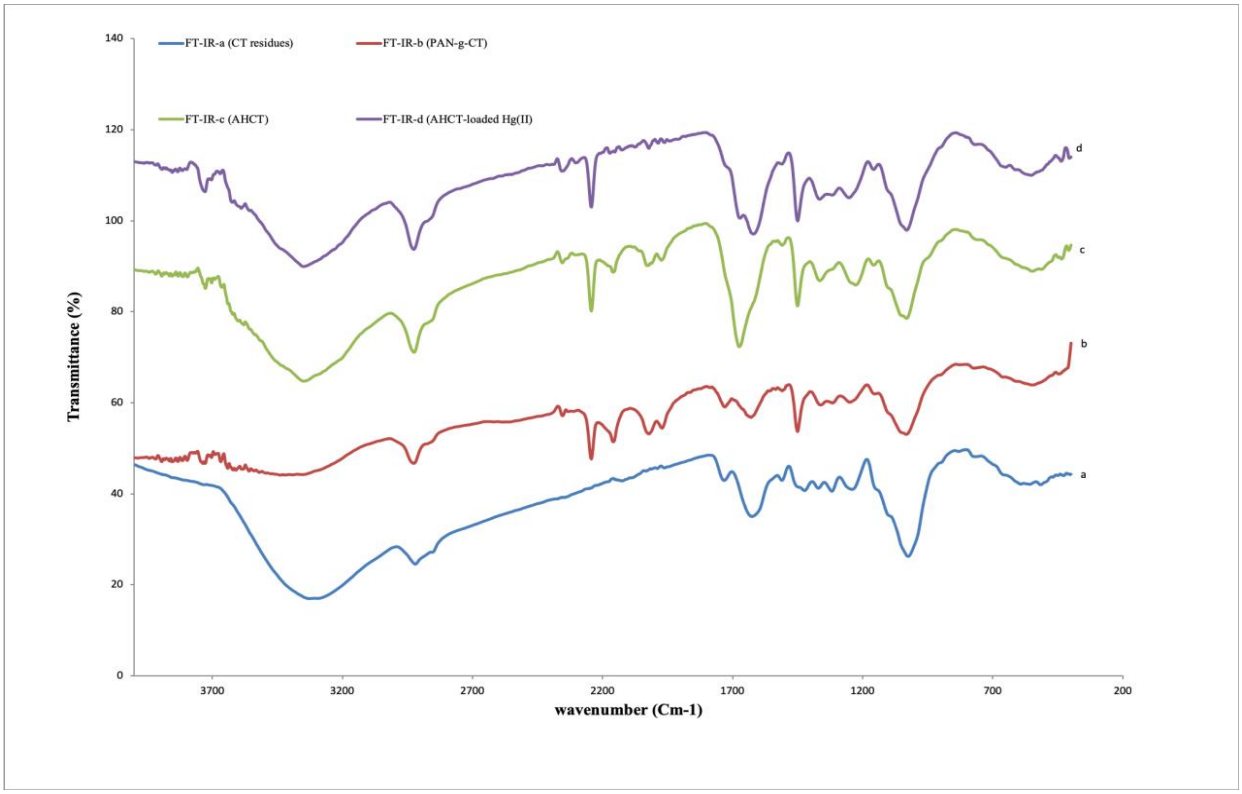

Fig. 1: FT-IR of CT residues (a), PAN-grafted-CT (b), AHCT (c) and AHCT-loaded-Hg(II) ions (d).

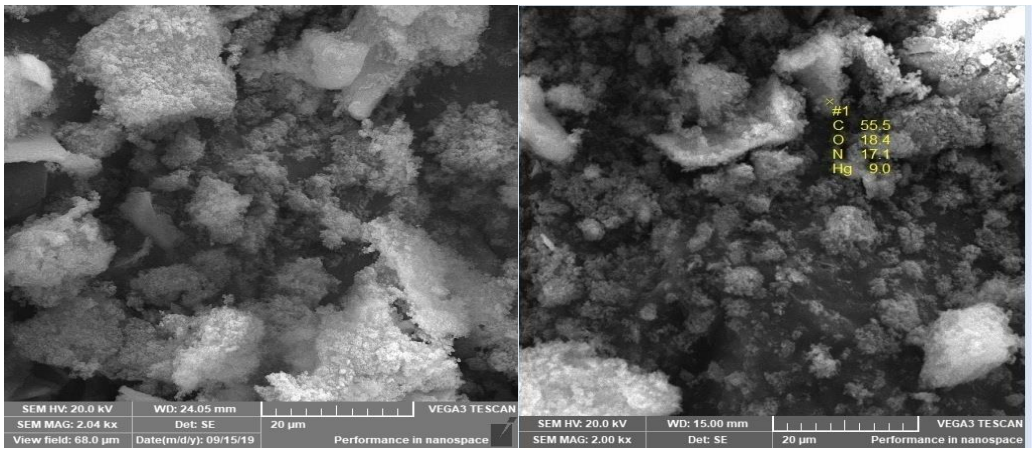

Fig. 2. SEM of AHCT residues (a) and AHCT -loaded Hg(II) ions (b).

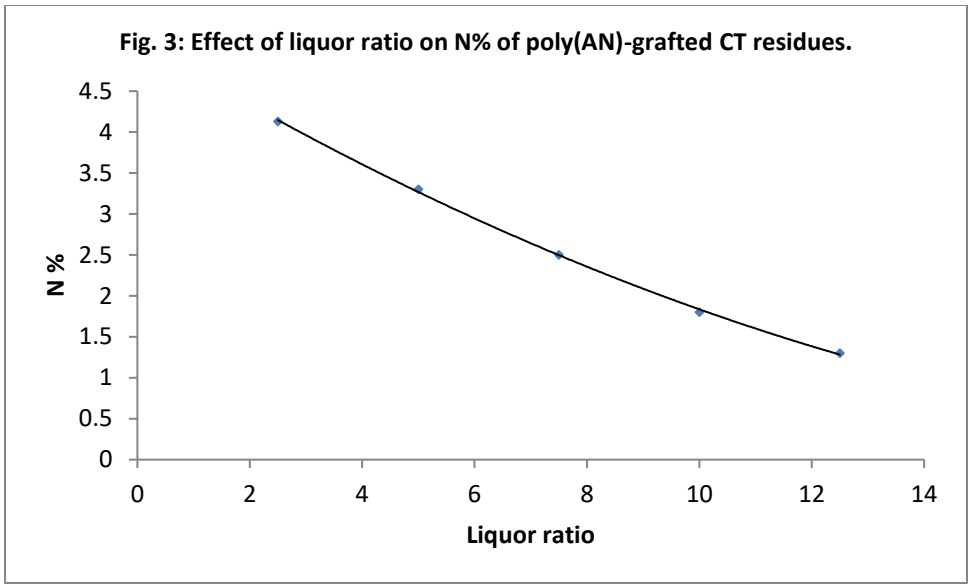

Grafting conditions: CT residues: 4g; AN, 22.811 mmol /l; CAN, 5 mmol /l; time, 2h; temperature, 60 ^{o}C.

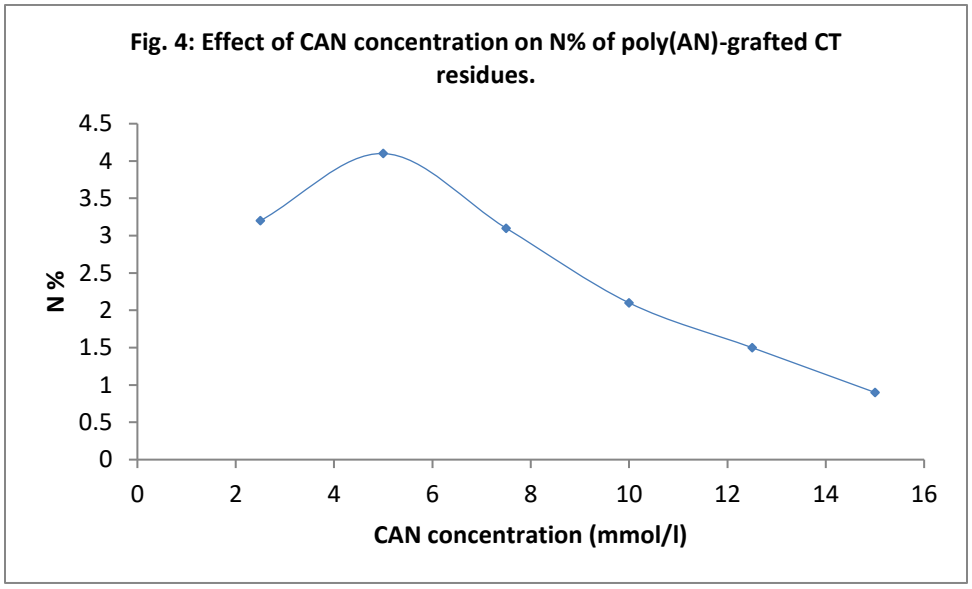

Grafting conditions: CT residues: 4g; AN, 22.811 mmol /l; L. R., 2.5; time, 2h; temperature, 60 ^{o}C.

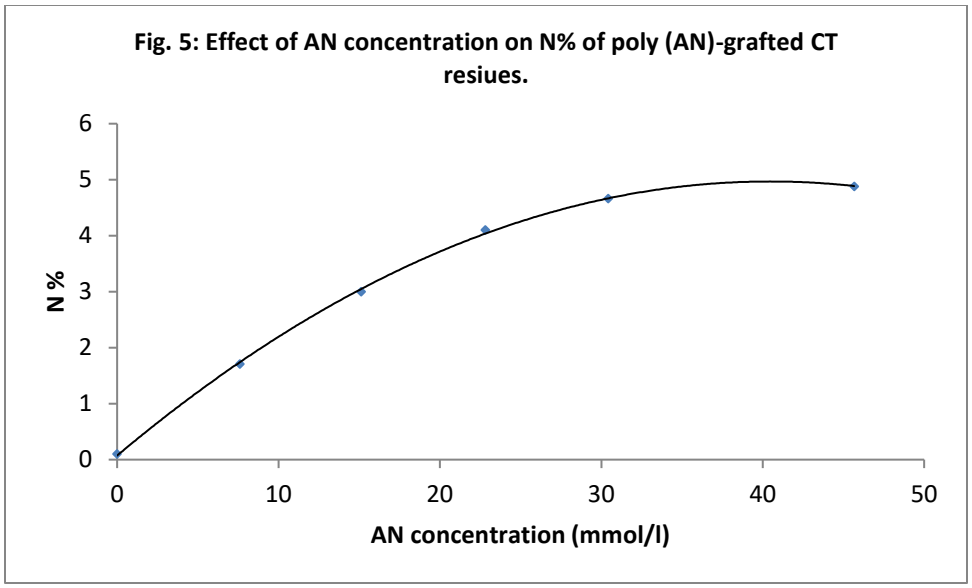

Grafting conditions: CT residues: 4g; CAN, 5 mmol /l; L.R, 2.5; time, 2h; temperature, 60 ^{o}C.

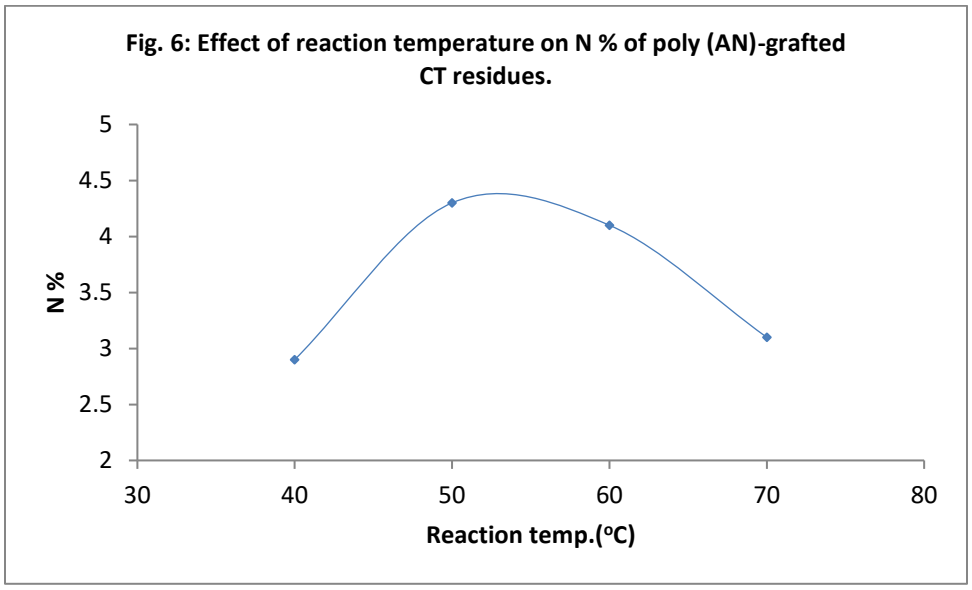

Grafting conditions: CT residues: 4g; AN, 22.811 mmol /l; CAN, 5 mmol/l; L. R., 2.5; time, 2h.

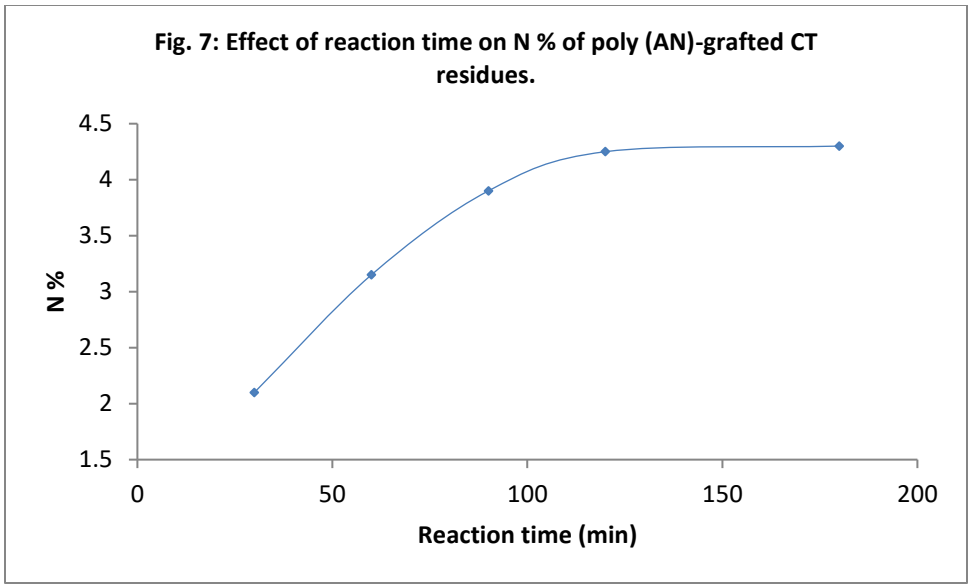

Grafting conditions: CT residues: 4g; AN, 22.811 mmol/l; CAN, 5 mmol/l; L.R, 2.5; reaction temp. 50 ^{o}C.

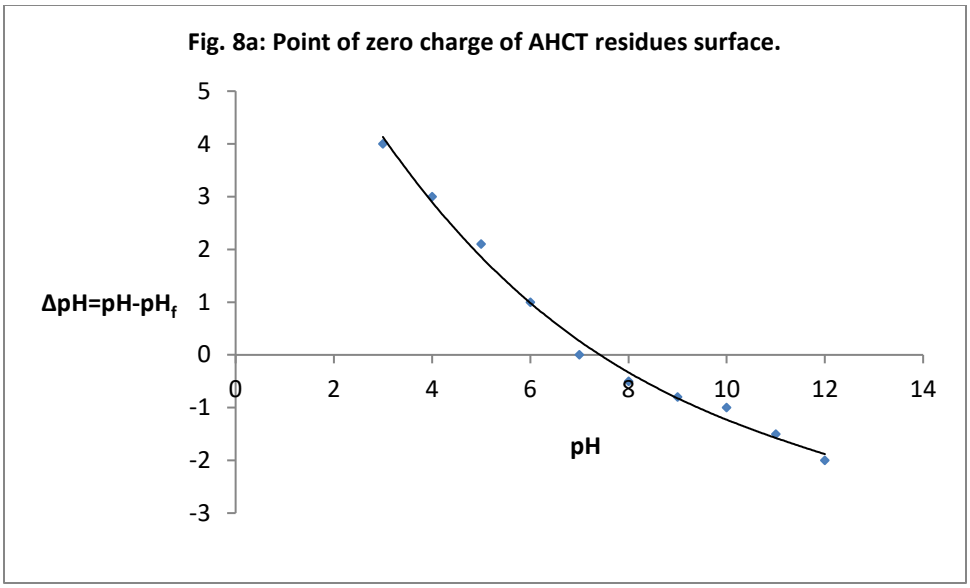

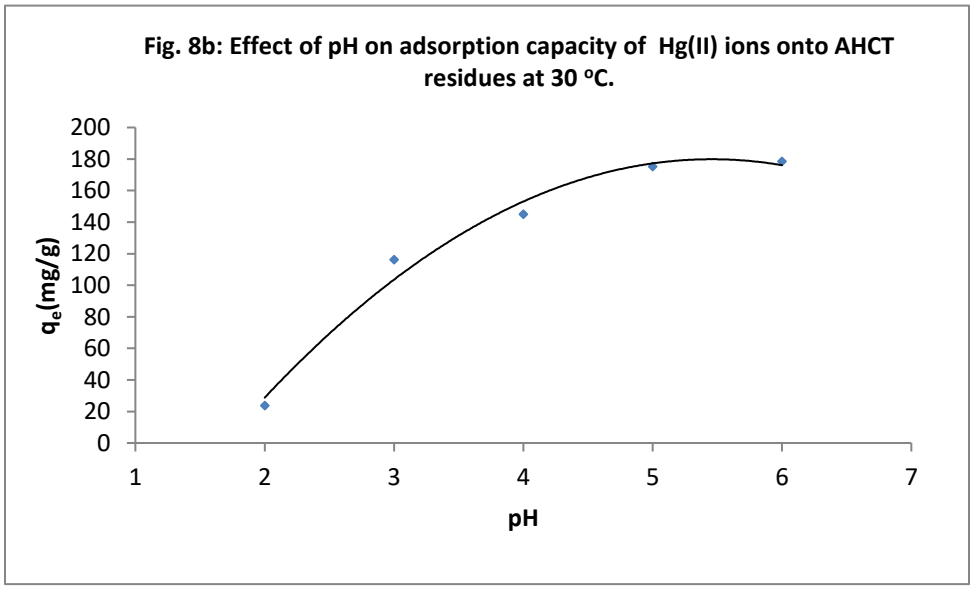

Reaction conditions: Hg(II) ion conc. ,300 mg/l ;adsorbent concentration, 0.3 g/l ;

contact time , 2h ; reaction temperature ,30 °C and particle size range,50-120 μm.

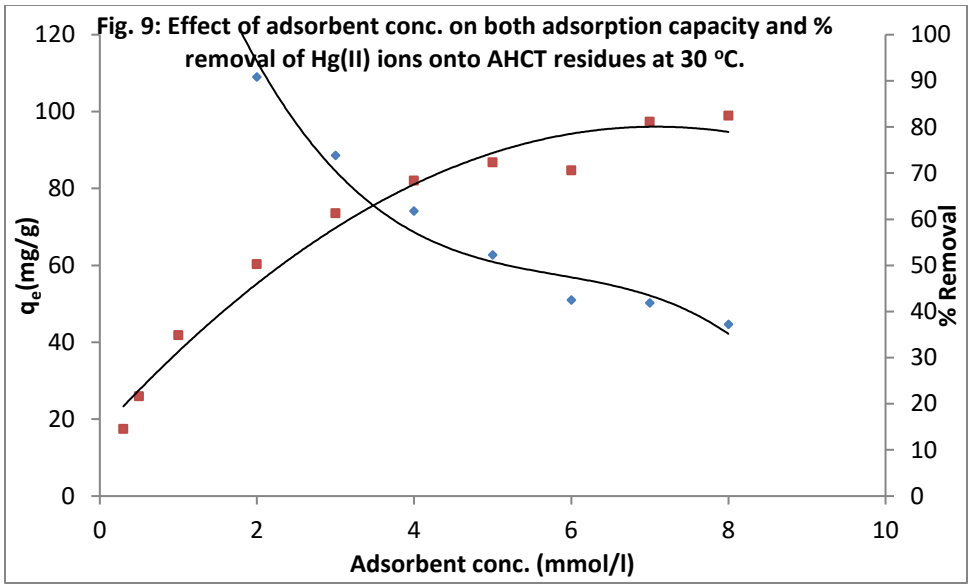

Reaction conditions: Hg(II) ion conc. ,300 mg/l ; pH, 5; contact time , 2h ; reaction temperature, 30 °C and particle size range,50-120 μm.

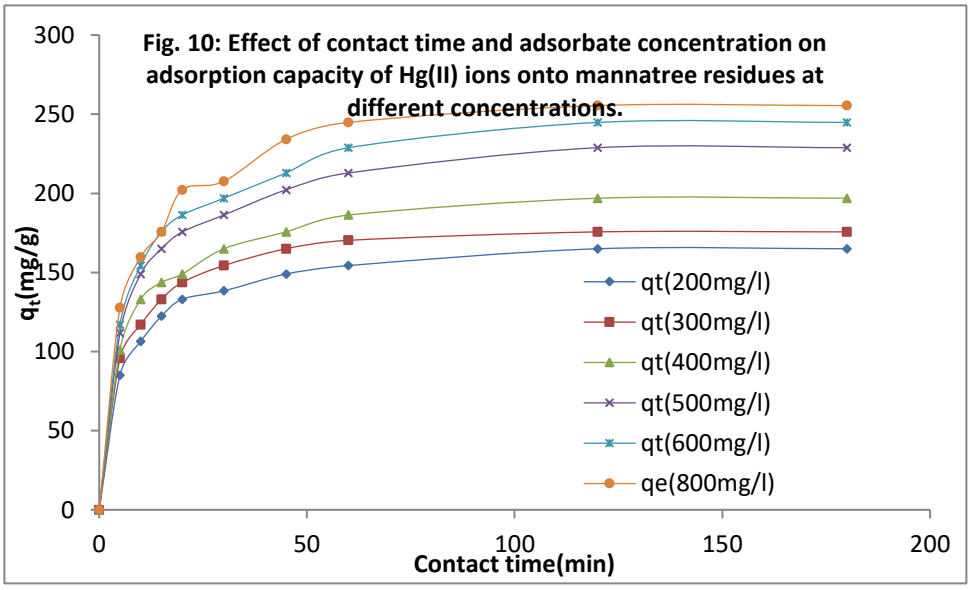

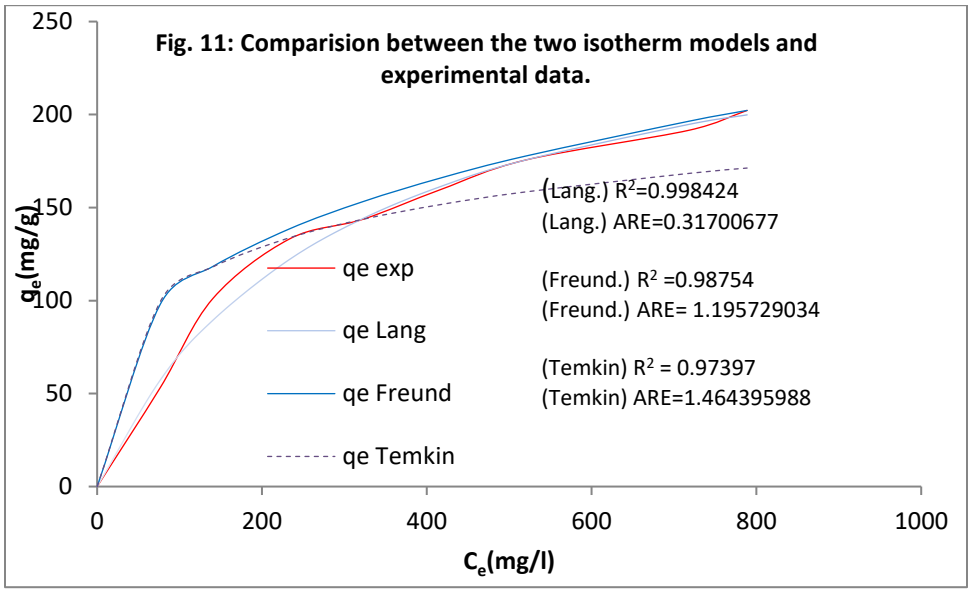
Fig. 11: Comparision between the two isotherm models and experimental data.
250
200
150
100
50
0
0
200
400
600
800
1000
q_e(mg/g)
C_e(mg/l)
qe exp
qe Lang
qe Freund
qe Temkin
(Lang.) R^2=0.998424
(Lang.) ARE=0.31700677
(Freund.) R^2 =0.98754
(Freund.) ARE= 1.195729034
(Temkin) R^2 = 0.97397
(Temkin) ARE=1.464395988

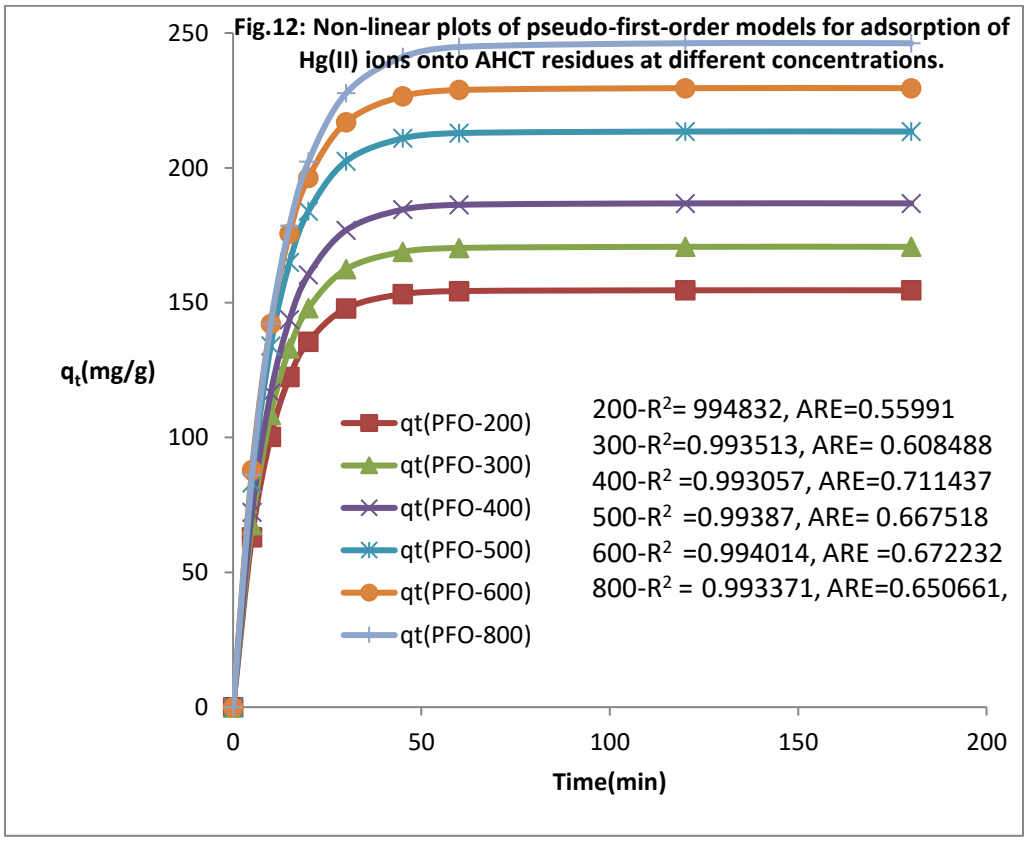
Fig.12: Non-linear plots of pseudo-first-order models for adsorption of Hg(II) ions onto AHCT residues at different concentrations.
250
200
150
100
50
0
0
50
100
150
200
q_t(mg/g)
Time(min)
qt(PFO-200)
qt(PFO-300)
qt(PFO-400)
qt(PFO-500)
qt(PFO-600)
qt(PFO-800)
200-R^2= 994832, ARE=0.55991
300-R^2=0.993513, ARE= 0.608488
400-R^2 =0.993057, ARE=0.711437
500-R^2 =0.99387, ARE= 0.667518
600-R^2 =0.994014, ARE =0.672232
800-R^2 = 0.993371, ARE=0.650661,

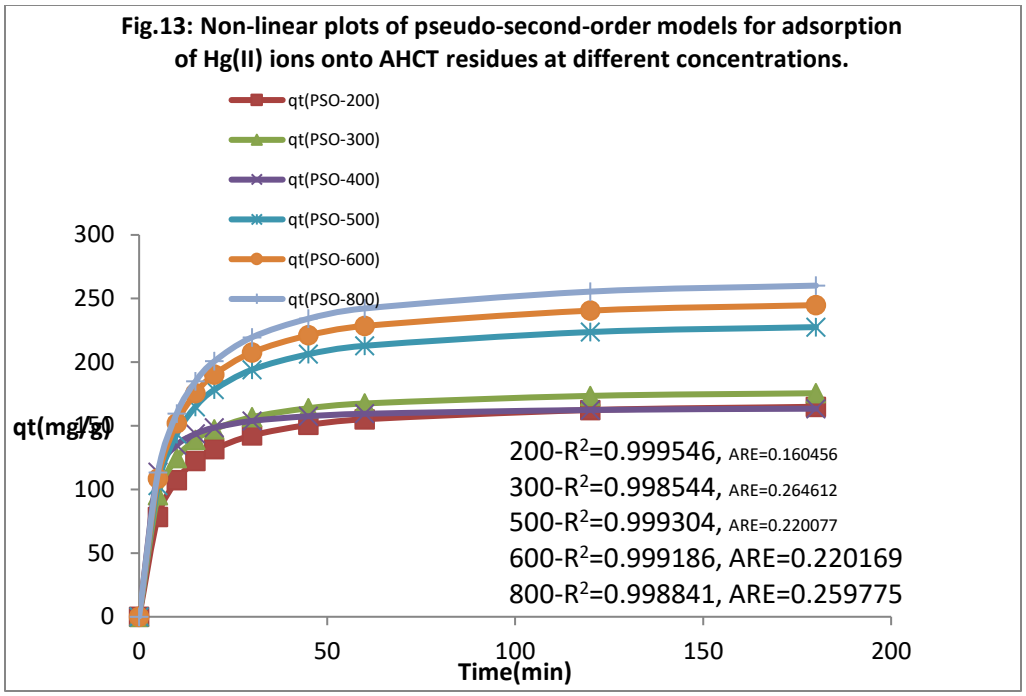
Fig.13: Non-linear plots of pseudo-second-order models for adsorption of Hg(II) ions onto AHCT residues at different concentrations.
qt(PSO-200)
qt(PSO-300)
qt(PSO-400)
qt(PSO-500)
qt(PSO-600)
qt(PSO-800)
qt(mg/g)
Time(min)
200-R2=0.999546, ARE=0.160456
300-R2=0.998544, ARE=0.264612
500-R2=0.999304, ARE=0.220077
600-R2=0.999186, ARE=0.220169
800-R2=0.998841, ARE=0.259775

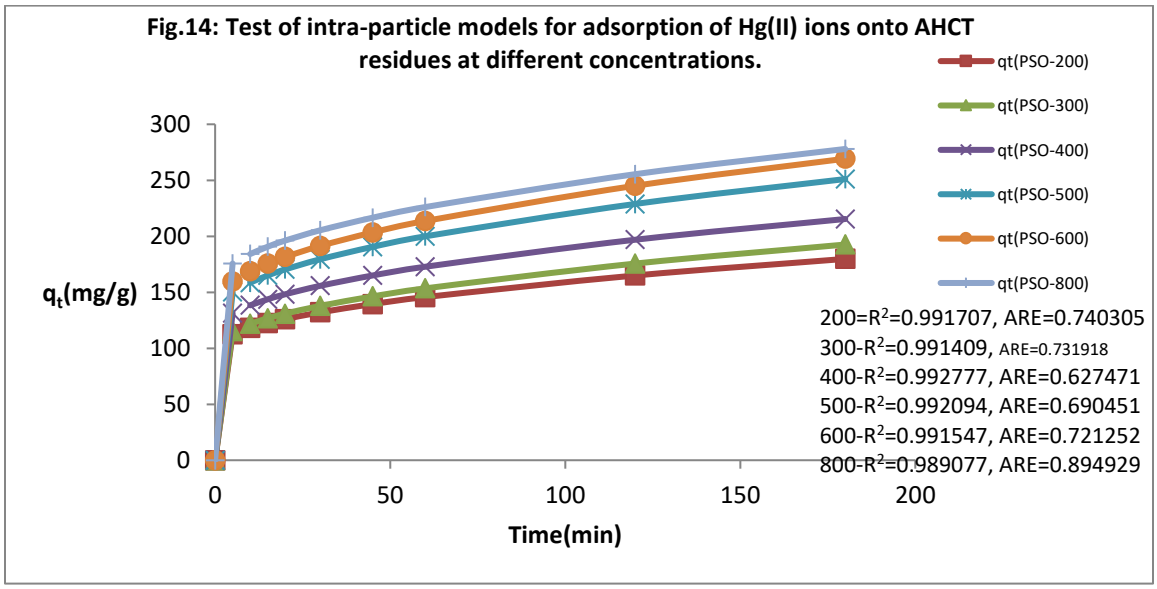
Fig.14: Test of intra-particle models for adsorption of Hg(II) ions onto AHCT residues at different concentrations.
qt(PSO-200)
qt(PSO-300)
qt(PSO-400)
qt(PSO-500)
qt(PSO-600)
qt(PSO-800)
qt(mg/g)
Time(min)
200=R2=0.991707, ARE=0.740305
300-R2=0.991409, ARE=0.731918
400-R2=0.992777, ARE=0.627471
500-R2=0.992094, ARE=0.690451
600-R2=0.991547, ARE=0.721252
800-R2=0.989077, ARE=0.894929